# DISK-PLANETS INTERACTIONS AND THE DIVERSITY OF PERIOD RATIOS IN KEPLER'S MULTI-PLANETARY SYSTEMS

CLEMENT BARUTEAU AND JOHN C. B. PAPALOIZOU
DAMTP, University of Cambridge, Wilberforce Road, Cambridge CB3 0WA, U.K.
Received 2013 January 4; accepted 2013 August 29

#### **ABSTRACT**

The Kepler mission is dramatically increasing the number of planets known in multi-planetary systems. Many adjacent planets have orbital period ratios near resonant values, with a tendency to be larger than required for exact first-order mean-motion resonances. This intriguing feature has been shown to be a natural outcome of orbital circularization of resonant planetary pairs due to star-planet tidal interactions. However, this feature holds in multi-planetary systems with periods longer than ten days, for which tidal circularization is unlikely to provide efficient divergent evolution of the planets orbits. Gravitational interactions between planets and their parent protoplanetary disk may instead provide efficient divergent evolution. For a planet pair embedded in a disk, we show that interactions between a planet and the wake of its companion can reverse convergent migration, and significantly increase the period ratio from a near-resonant value. Divergent evolution due to wake-planet interactions is particularly efficient when at least one of the planets opens a partial gap around its orbit. This mechanism could help account for the diversity of period ratios in Kepler's multiple systems comprising super-Earth to sub-jovian planets with periods greater than about ten days. Diversity is also expected for pairs of planets massive enough to merge their gap. The efficiency of wake-planet interactions is then much reduced, but convergent migration may stall with a variety of period ratios depending on the density structure in the common gap. This is illustrated for the Kepler-46 system, for which we reproduce the period ratio of Kepler-46b and c.

Keywords: accretion, accretion disks — hydrodynamics — methods: numerical — planetary systems: formation — planetary systems: protoplanetary disks

### 1. INTRODUCTION

Planetary astrophysics is undergoing an epoch of explosive growth driven by the discovery of about 850 exoplanets in two decades. Continuous improvement in detection techniques will uncover many more planets in the near future which are too small or too far from their host star to be detected at present. Observations suggest that planet formation is ubiquitous, with more than 40% of nearby Sun-like stars harboring at least one planet less massive than Saturn (Mayor et al. 2009). These prolific discoveries have revealed the amazing diversity of exoplanetary systems and indicated that planets may form under a wide range of conditions and have considerable mobility.

The diversity of exoplanets has been particularly high-lighted by the Kepler's space mission. To date, Kepler has detected over 2300 planet candidates (Batalha et al. 2013), from which more than a hundred are confirmed planets (http://kepler.nasa.gov). About one third of Kepler's candidates are associated with multiple transiting systems and the vast majority of them are expected to be real multiplanetary systems (Lissauer et al. 2012). Some of these systems show remarkable properties, like the five coplanar, alternating rocky and icy planets orbiting Kepler-20 in less than 80 days (Gautier et al. 2012). Interactions between planets and their parent protoplanetary disk are likely to have played a major role in shaping such compact system.

A striking feature of Kepler's multi-planetary systems is the large number of planet pairs far from mean-motion resonances (hereafter MMR, Lissauer et al. 2011). Planet pairs near resonances show some tendency to have period ratios slightly greater than resonant values (see Figure 1; period ratios are defined as the outer planet's orbital period divided by the inner planet's). For instance, there are almost twice as many planet pairs with period ratios between 2.0 and 2.1 than between 1.9 to 2.0. This intriguing feature could naturally arise from tidal orbital circularization of close-in resonant planet pairs (Papaloizou 2011; Lithwick & Wu 2012; Batygin & Morbidelli 2013). However, as stressed by the histograms in Figure 1, the same trend holds for planet pairs where the orbital period of the inner planet exceeds 10 days, most particularly near first-order resonances. For such systems, tidal circularization is unlikely to have caused significant divergent evolution of the planets orbits, as shown in Section A of the appendix.

An example of a planetary system with a period ratio slightly greater than resonant is the Kepler-46 system (previously known as KOI-872). The 0.9 Solar-mass star is surrounded by a  $0.8R_{\rm J}$  transiting planet on a 33.6 day period (Kepler-46b). Large transit time variations (TTV) of Kepler-46b are caused by the presence of an outer planet, Kepler-46c, whose mass  $(0.37M_{\rm J})$  and orbital period  $(57.0 \, {\rm days})$  have been determined by Nesvorný et al. (2012). The same authors have also reported the detection of a  $1.7R_{\oplus}$  planet candidate on a 6.8 day period (Kepler-46d, not yet confirmed). The main properties of the Kepler-46 planetary system are summarized in Table 1. The low-eccentricity and quasi-coplanar orbits in this system suggest that the planets reached their present location most probably through disk-planet interactions. Still, the ratio or orbital periods between Kepler-46c and Kepler-46b is  $\approx 1.696$ , which is slightly greater than 5/3. Capture in the 5:3 MMR is not a natural outcome of planet migration driven by disk-planet interactions. It requires a rate of convergent migration that is large enough to cross the 2:1 MMR, but not too large so that the planets do not reach their 3:2 MMR.

 Table 1

 Kepler-46 planetary system (Nesvorný et al. 2012)

	Mass or radius	Period [days]	Eccentricity
Kepler-46	$0.9M_{\odot}$	_	_
Kepler-46da	$\approx 1.7R_{\oplus}$	6.8	0 (assumed)
Kepler-46b	$\approx 0.8R_{\rm J}$	33.6	$\leq 0.02$
Kepler-46cb	$0.37M_{\rm J}$	57.0	$\approx 0.015$

<sup>&</sup>lt;sup>a</sup>Unconfirmed.

Capture into a second-order resonance also requires small but not zero eccentricities, which disk-planet interactions tend to damp quite efficiently. Should disk-planet interactions have led Kepler-46b and Kepler-46c to reach their 5:3 MMR, it is unclear how their period ratio would have then increased to their present value.

The initial motivation of this work is to investigate under what circumstances disk-planets interactions may account for the orbital period ratio between Kepler-46c and Kepler-46b. In Section 2, we present results of hydrodynamical simulations modeling the early evolution of both planets as they were embedded in their parent protoplanetary disk. These Saturn-mass planets are expected to open a partial gap around their orbit. A rapid convergent migration causes the planets to merge their gap and to evolve into a common gap. The planets' convergent migration is found to stall with period ratios between 1.5 and 1.7, depending on the disk's density profile inside the common gap. The observed period ratio can be reproduced without the planets being in resonance. Furthermore, we show that disk-driven migration of partial gapopening planets may lead to significant divergent evolution of planet pairs over typical disk lifetimes. Such divergent evolution is shown to arise from the interaction between planets and the wakes of their companions. This mechanism is illustrated for super-Earth-mass planets in Section 3 with both hydrodynamical simulations and customized three-body integrations. Divergent evolution of gap-opening planet pairs mediated by wake-planet interactions could partly account for the diversity of period ratios in Kepler's multi-planetary systems. Concluding remarks are provided in Section 4.

## 2. HYDRODYNAMICAL SIMULATIONS OF THE KEPLER-46 PLANETARY SYSTEM

We model in this section the early evolution of the Kepler-46 planetary system when the planets were embedded in their parent protoplanetary disk. Our study does not address the formation of the planets. We focus instead on the planets orbital evolution due to disk-planet and planet-planet interactions. Two-dimensional hydrodynamical simulations of disk-planets interactions were carried out using the code FARGO (Masset 2000). The physical model and numerical setup of the hydrodynamical simulations are described in Section 2.1. Results of simulations follow in Section 2.2.

## 2.1. Physical model and numerical setup

Disk model— We adopt a two-dimensional disk model for the protoplanetary disk in which the planets orbiting Kepler-46 formed. Disk-planets interactions determine the rate of convergent migration of the planets and the damping rate of their eccentricity. Both quantities are sensitive to the disk's surface density, temperature, turbulent viscosity and radiative properties. The parameter space is therefore particularly large, and the need to assess the planets' orbital evolution over typically

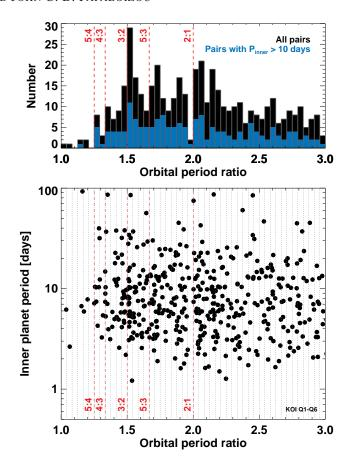


**Figure 1.** Bottom: ratio of orbital periods of all planet pairs among Kepler's candidate multi-planetary systems detected from Quarters 1 to 6 (x-axis) versus the orbital period of the inner planet in each pair (in days, y-axis). Bins are 1/24 wide. From left to right, vertical dashed lines show the location of the 5:4, 4:3, 3:2, 5:3 and 2:1 mean-motion resonances. Top: histograms of the orbital period ratio for all planet pairs (black), and for planet pairs where the inner planet's period is greater than 10 days. Data were extracted from http://planetquest.jpl.nasa.gov/kepler/.

a thousand planet orbits has led us to make simplifying assumptions for the disk model and to fix some of the disk parameters.

Disk self-gravity is discarded given the low disk masses adopted in this work (the Toomre-Q parameter associated with the unperturbed density profile does not go below 7). A locally isothermal equation of state is used where the vertically-integrated pressure P and density  $\Sigma$  satisfy  $P = \Sigma c_s^2$ , with the sound speed  $c_s$  being specified as a fixed function of the cylindrical radius r. The sound speed is related to the disk's pressure scale height H through  $H = c_s/\Omega_K$  with  $\Omega_K$  the Keplerian angular velocity. The (fixed) temperature profile is taken proportional to  $r^{-1}$  so that the disk's aspect ratio h = H/r is uniform. We take the standard value h = 0.05. A locally isothermal equation of state is generally not appropriate to model the migration of an embedded lowmass planet, as it underestimates the magnitude of the corotation torque that the planet experiences from the disk; see Baruteau & Masset (2013) for a recent review on planet migration. This is not an issue in this study, however, since we consider partial gap-opening planets for which the corotation torque has a rather weak effect on migration. This may be quantified through the dimensionless parameter  $q/h^3$  (q denotes the planet-to-star mass ratio) which is  $\geq 2$  in our simu-

<sup>&</sup>lt;sup>b</sup>Inferred from TTV signal of Kepler-46b.

lations. This lower limit implies that the direction and speed of planet migration are weakly sensitive to the choice for the equation of state (Kley & Crida 2008).

The effects of turbulence are modeled by a constant shear kinematic viscosity v. We take  $v = 1.1 \times 10^{-5}$  in standard code units (defined below) which translates into a viscous alpha parameter  $\alpha = 4.5 \times 10^{-3}$  at the initial location of the inner planet. This value of  $\alpha$  is typical of the magnetically active regions of protoplanetary disks with magnetohydrodynamic turbulence driven by the magneto-rotational instability. The present orbital periods of the planets in the Kepler-46 system imply that the planets have probably interacted with such active regions in their parent disk. Note, however, that the disk's magnetic field is not included in our simulations. We also point out that the planets that we consider are of large enough mass so that small-scale turbulent fluctuations can be safely ignored when modeling the interaction with their parent disk. In other words, the viscous diffusion approximation is expected to be a reasonable approximation for the large planet masses we consider (Nelson & Papaloizou 2003; Baruteau et al. 2011).

The disk is set up in radial equilibrium, with the centrifugal acceleration and the radial acceleration related to the pressure gradient balancing the gravitational acceleration due to the central star. The initial gas surface density is taken proportional to  $r^{-1/2}$ . Its value at the initial location of the inner planet is taken as a free parameter, which we denote by  $\Sigma_0$ .

Planet parameters— We model the orbital evolution of the outer two planets in the Kepler-46 system: Kepler-46b (hereafter refereed to as the inner planet) and Kepler-46c (as the outer planet). The  $1.7R_{\oplus}$  unconfirmed planet candidate with a period of 6.8 days is assumed to have had a negligible impact on the orbital evolution of Kepler-46b and Kepler-46c. The planets are assumed to have already formed at the beginning of our simulations, they therefore take their present mass. Kepler-46b has a physical radius  $\approx 0.8R_{\rm I}$ . However, its mass could not be constrained from TTV; see Nesvorný et al. (2012). The mass-radius diagram of exoplanets detected by transiting methods indicates that the mass of Kepler-46b most probably lies between  $0.2M_{\rm I}$  and  $0.6M_{\rm J}$ . Its planet-to-primary mass ratio ( $q_{\rm inner}$ ) is therefore varied in the range  $[2.2\times10^{-4}, 6.6\times10^{-4}]$ . The TTV signal of Kepler-46b constrains the mass of Kepler-46c to be  $\approx 0.37 M_{\rm J}$  (Nesvorný et al. 2012). The planet-to-primary mass ratio of Kepler-46c is thus fixed to  $q_{\text{outer}} = 4 \times 10^{-4}$ . The initial orbital radius of Kepler-46b,  $r_{inner}$ , is taken to be the code's unit of length. That of Kepler-46c is arbitrarily set to  $r_{\text{outer}} = 1.8 r_{\text{inner}}$ , so that the ratio of orbital periods  $\approx 2.4$  initially. For the disk aspect ratio and viscosity taken in our study, the two planets are expected to open a partial gap around their orbit (Lin & Papaloizou 1993; Crida et al. 2006).

Numerical setup— The hydrodynamical equations are solved in a cylindrical coordinate system  $\{r, \varphi\}$  centered on to the star with  $r \in [0.2-2.6]r_{\rm inner}$  and  $\varphi \in [0,2\pi]$ . The computational grid has  $N_{\rm r}=400$  zones evenly spaced along the radial direction and  $N_{\rm s}=800$  azimuthal sectors. The frame rotates with the Keplerian frequency at the inner planet's location, and the indirect terms that account for the acceleration of the central star by the disk and the planets are included in the equations of motion. A standard outflow

boundary condition is taken at the grid's inner edge, while damping is used in a so-called wave killing-zone extending from r=2.2 to r=2.6 (disk quantities are damped towards their instantaneous axisymmetric profile). To avoid a violent relaxation of the disk due to the sudden introduction of the planets, the mass of the planets is gradually increased over 10 orbital periods. The gravitational potential of the planets is smoothed over a softening length,  $\varepsilon$ , equal to 0.6H with H evaluated at the planets location. The calculation of the force exerted by the disk on the planets excludes the content of the planets' circumplanetary disk, the size of which being about 60% of the planets' Hill radius (Crida et al. 2009). The Hill radius of each planet is resolved by about 10 grid cells along each direction initially.

Code units— Results of simulations are expressed in the standard units of disk-planet calculations: the mass unit is the mass of the central star (denoted by  $M_{\star}$  and equal to  $0.9 M_{\odot}$  for the Kepler-46 system). The length unit is the initial orbital radius of the inner planet ( $r_{\rm inner}$ ), and the time unit is the initial orbital period of the inner planet ( $T_{\rm orb}$ ) divided by  $2\pi$ . Whenever time is expressed in orbits, it refers to the orbital period at the initial location of the inner planet.

#### 2.2. Results of hydrodynamical simulations

The free parameters in our simulations are the mass of the inner planet and the initial surface density of the disk. Both quantities determine the rate of convergent migration and the evolution of the orbital eccentricities. We consider three different masses for the inner planet: 0.2M<sub>J</sub>, 0.4M<sub>J</sub> and 0.6M<sub>J</sub> (recall that the mass of the outer planet is fixed at  $0.37M_{\rm J}$ ). For each planet mass, a set of 9 simulations was carried out varying  $\Sigma_0$ , the unperturbed surface density at the initial orbital radius of the inner planet. We took  $\Sigma_0$  in the range  $[2 \times 10^{-4}, 10^{-3}]$ , which corresponds to an initial disk mass between  $3.5 \times 10^{-3} M_{\star}$  and  $1.8 \times 10^{-2} M_{\star}$ . Typical outcomes of the simulations are described in Section 2.2.1. We find that disk-planets interactions may lead to significant divergent evolution of the planet orbits, which we interpret in Section 2.2.2. To obtain evolution of the planets' orbital elements to a steady state, a simple model for disk dispersal is included and its results presented in Section 2.2.3. The robustness of our results to varying some physical and numerical parameters is discussed in Section B of the appendix.

#### 2.2.1. A few illustrative cases

Figure 2 displays typical outcomes of our hydrodynamical simulations of the Kepler-46 system. From left to right in the figure we show the time evolution of the planets' semi-major axes, orbital period ratio, eccentricities and resonant angles. Here  $\lambda_{i,o}$  and  $\omega_{i,o}$  denote the mean longitude and longitude of periastron, with the subscripts i and o referring to the inner and outer planets, respectively.

The top row shows results with  $M_{\rm inner} = 0.4 M_{\rm J}$  and  $\Sigma_0 = 3 \times 10^{-4}$ . As the planets progressively clear a partial gap around their orbit, convergent migration does not occur at a constant rate. In particular, the inward migration of the outer planet slightly accelerates at early times due to a stage of type III migration (Masset & Papaloizou 2003) before slowing down upon approaching the 2:1 MMR with the inner planet. The planets are locked in the 2:1 MMR from about 300 orbits onwards, as can be seen from the libration of the resonant angles associated with this resonance. The reso-

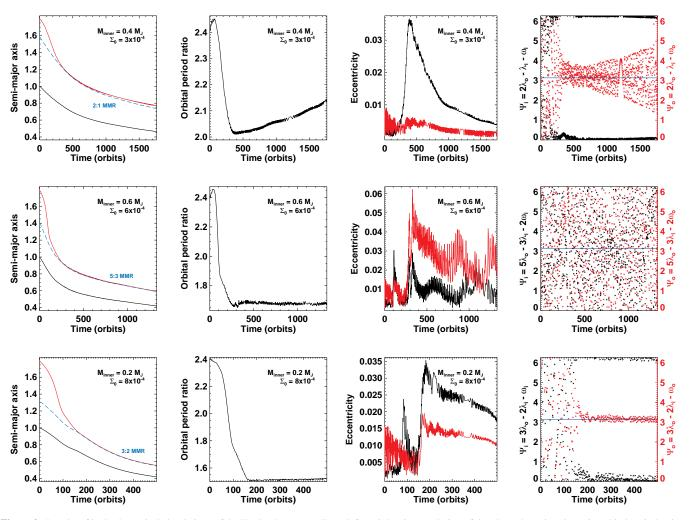
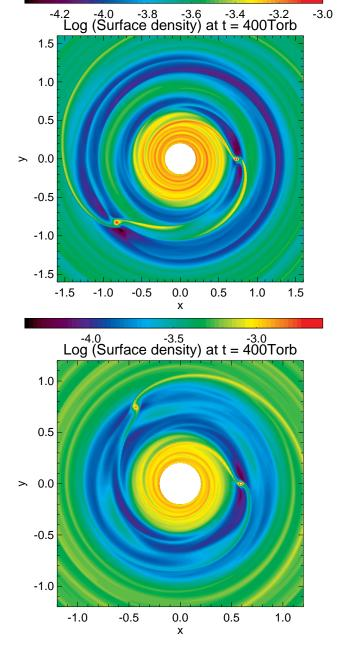


Figure 2. Results of hydrodynamical simulations of the Kepler-46 system. From left to right: time evolution of the planets' semi-major axis, orbital period ratio, eccentricity and of the resonant angles relevant to the planets' period ratio (the horizontal line marks  $\pi$ ). Each row corresponds to a different simulation, for which the inner planet's mass ( $M_{\text{inner}}$ ) and the disk's unperturbed surface density at r=1 ( $\Sigma_0$ ) are indicated in the top-right corner of the panels. The outer planet's mass is 0.37  $M_{\text{J}}$ . The location of some mean-motion resonances (MMR) are displayed by dashed curves in the semi-major axes panels. The first row shows an example of convergent migration towards the 2:1 MMR followed by rapid divergent evolution. The second row shows a case where convergent migration stalls with an orbital period ratio near 1.7 (as determined by TTV). In the third row, capture into the 3:2 MMR is followed by slow divergent evolution.

nance capture increases the inner planet's eccentricity to about 0.035. The increase in the outer planet's eccentricity is much more modest, reaching about  $5 \times 10^{-3}$ , even though the mass ratio of the planets is near unity. This modest increase in the outer planet's eccentricity arises from the contribution of the indirect term nearly cancelling the contribution from the direct term to the term that is first order in the eccentricities in the development of the disturbing function, which governs the response of the outer planet at a 2:1 MMR (see, e.g., Murray-Clay & Chiang 2005; Papaloizou & Terquem 2010). Damping of the eccentricities follows from the gravitational interaction with the background gas disk. Interestingly, the ratio of orbital periods rises from 2.02 to 2.15 in only 1500 orbits, while the eccentricities are damped. The physical origin of this divergent evolution is discussed in Section 2.2.2. Note that resonant coupling is maintained throughout this divergent evolution, the width of the 2:1 MMR increasing as the eccentricities decrease.

The second row of panels in Figure 2 displays results for  $M_{\rm inner} = 0.6 M_{\rm J}$  and  $\Sigma_0 = 6 \times 10^{-4}$ . This case is particularly interesting as it shows that convergent migration may stall

with an orbital period ratio very close to the observed value  $(\approx 1.7)$ . The accelerating inward migration of the outer planet is particularly visible in the first 100 orbits. This runaway migration is fueled by the dense gas region located between the two planet gaps. This dense material is continuously funneled beyond the outer planet's orbit upon embarking on horseshoe U-turns with respect to the outer planet. The density between the two planet gaps therefore decreases, and so does the migration rate of the outer planet. Convergent migration then proceeds at a slower pace and the planets end up merging their gap, thereby forming a common gap in the disk. This is illustrated in Figure 3, which compares the disk's surface density at 400 orbits for the two aforementioned simulations which have  $M_{\rm inner}=0.4M_{\rm J}$  and  $\Sigma_0=3\times 10^{-4}$  (top panel), and  $M_{\rm inner}=0.6M_{\rm J}$  and  $\Sigma_0=6\times 10^{-4}$  (bottom panel). While in the former case a narrow ring of gas is left between the two planet gaps, the latter case shows that both planets end up in a common gap. Back to the second row of panels in Figure 2, we see that the orbital period ratio remains approximately stationary from about 400 orbits, and so do the eccentricities. The time-averaged eccentricity of the inner planet is close to



**Figure 3.** Disk's surface density at 400 orbits for  $M_{\rm inner} = 0.4 M_{\rm J}$  and  $\Sigma_0 = 3 \times 10^{-4}$  (top), and for  $M_{\rm inner} = 0.6 M_{\rm J}$  and  $\Sigma_0 = 6 \times 10^{-4}$  (bottom). The outer planet's mass is  $M_{\rm outer} = 0.37 M_{\rm J}$ .

0.01; that of the outer planet is  $\approx$  0.025. These values are consistent, albeit slight larger than those inferred from observations (see Table 1). Note from the critical angles that the planets are not locked in the 5:3 MMR.

Lastly, the third row of panels in Figure 2 is for  $M_{\rm inner} = 0.2 M_{\rm J}$  and  $\Sigma_0 = 8 \times 10^{-4}$ . Here, convergent migration is rapid enough that the planets approximately reach the nominal location of their 3:2 MMR (the minimum value of the period ratio is 1.508 at 170 orbits). The planet eccentricities increase to about 0.03 (inner planet) and 0.015 (outer planet). Subsequent damping of the eccentricities occurs along with a slight divergent evolution of the planets. The rate of divergent evolution is much reduced compared to the 2:1 MMR case shown

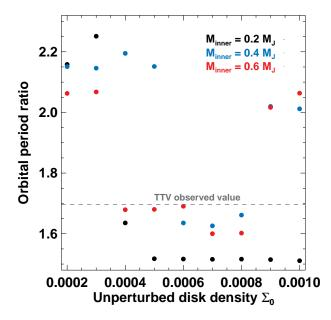


**Figure 4.** Summary of the results of hydrodynamical simulations for Kepler-46: ratio of orbital periods versus the unperturbed disk's surface density at the initial location of the inner planet ( $\Sigma_0$ ). Results are shown for the three masses assumed for the inner planet (Kepler-46b).

in the top row of panels in Figure 2. We will analyse this result further in Section 2.2.2. We also point out that no steady-state has been reached at the end of the simulation. For this simulation, as for all simulations of the Kepler-46 system, results are shown until the inner planet reaches  $r \sim 0.4$ , below which the proximity of the grid's inner edge (at r = 0.2) starts affecting the planets orbital evolution.

The final period ratio obtained in all our simulations is displayed in Figure 4 as a function of  $\Sigma_0$  for the three masses assumed for Kepler-46b. By final period ratio, we mean either its value obtained at the end of the simulation (after between 1500 and 2000 planet orbits), or that obtained when the inner planet's orbital radius falls below r = 0.4. Figure 4 highlights the three major outcomes of our simulations: (i) capture in 2:1 MMR generally followed by rapid divergent evolution, (ii) capture in 3:2 MMR followed by slow divergent evolution, and (iii) convergent migration stalling with a period ratio between 1.6 and 1.7, depending on the disk's density distribution inside the planets' common gap. Several simulations can reproduce the observed period ratio of Kepler-46b and Kepler-46c. The best agreement with observations is obtained for  $M_{\text{inner}} = 0.6 M_{\text{J}}$ , our upper mass value. This mass would imply a mean density for Kepler-46b about 20% larger than Jupiter's (that is, about  $1.6 \text{ g cm}^{-3}$ ).

#### 2.2.2. Disk-driven repulsion of a planet pair

The results of hydrodynamical simulations in Section 2.2.1 show that the orbital period ratio of two partial gap-opening planets may increase from a near resonant value. This divergent evolution is reminiscent of the late evolution of short-period planet pairs through star-planet tidal interactions. In that case, tidal circularization causes a slow divergent evolution of the orbits (Papaloizou & Terquem 2010; Papaloizou 2011; Lithwick & Wu 2012; Batygin & Morbidelli 2013), a mechanism known as tidally-driven resonant repulsion (Lithwick & Wu 2012). It is based on energy dissipation of

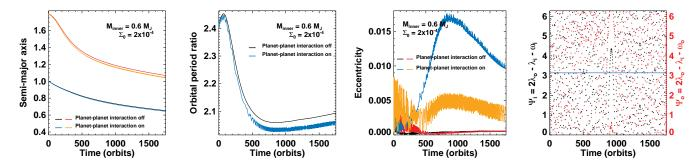


Figure 5. Time evolution of the semi-major axes, the orbital period ratio, the eccentricities and the 2:1 resonant angles for  $M_{\text{inner}} = 0.6M_{\text{J}}$  and  $\Sigma_0 = 2 \times 10^{-4}$ . Two situations are compared: (i) the planets do not feel each other's gravity (planet-planet interaction off) and (ii) the planets feel each other's gravity (planet-planet interaction on; our fiducial case). The resonant angles are those obtained with planet-planet interaction off.

the planet pair while its total angular momentum remains constant (Papaloizou 2011).

Do we have an analogous resonant repulsion mechanism due to disk-planets interactions? To address this question, it is instructive to first look at the evolution of two embedded planets that do not interact gravitationally. In Figure 5 we compare the results of two hydrodynamical simulations: one in which the gravitational interaction between the planets is switched off (both the direct and the indirect interaction terms are discarded) and another where the planet-planet interaction is fully accounted for. The inner planet's mass is  $M_{\rm inner} = 0.6 M_{\rm J}$  and the initial disk surface density at r = 1is  $\Sigma_0 = 2 \times 10^{-4}$ . The other disk and planet parameters are those described in Section 2.1. When planet-planet interactions are on, capture into the 2:1 MMR is followed by rapid divergent evolution and damping of the eccentricities. This case is similar to that presented in the top row of panels in Figure 2. Quite surprisingly, we see that a very similar divergent evolution is also obtained when planet-planet interactions are switched off, while the planets are not resonantly coupled (the resonant angles do not librate) and their eccentricities take vanishingly small stationary values. This comparison highlights that, when disk-planet interactions are considered, eccentricity damping is not necessarily responsible for the planets divergent evolution. The divergent evolution of a planet pair may instead be driven by changes to the disk-planet interaction brought about through the proximity of the planets to each other, such as the development of an interaction between each planet and the wake of its companion. We argue below that the damping of the eccentricities can actually be a consequence of divergent evolution driven by wake-planet interaction.

Before describing the process of wake-planet interaction in more detail, we briefly report that, in some other simulations, not illustrated here, with planet-planet interactions switched off, a tiny increase in the orbital eccentricities is observed when the orbital period ratio takes near resonant values. Eccentricities may reach a few  $\times 10^{-3}$  before being damped by the disk. Although this is a small effect, it suggests that planets could be weakly resonantly coupled through interaction with the wakes and/or the circumplanetary disk of their companions. In our simulations, the mass of the circumplanetary disks does not exceed one percent of the planets mass.

Wake-planet interactions— The results of simulations shown in Figure 5 make clear that disk-driven divergent evolution of

a planet pair is not necessarily driven by eccentricity damping and it may continue to operate even when the eccentricities are very small. We here indicate how the interaction between a planet and the wake of its companion could act as a driving mechanism for divergent evolution. Consider for instance the inner planet. Its outer wake carries positive fluxes of angular momentum and energy. A fraction of this angular momentum flux can be deposited in the coorbital region of the outer planet through the dissipation of shocks, and then transferred to the outer planet via an effective positive corotation torque (see Podlewska-Gaca et al. 2012). Associated with the angular momentum flux  $F_{\rm I}$  deposited in the coorbital region of the outer planet is an energy flux  $F_E = n_i F_J$ , where  $n_i$  denotes the inner planet's mean motion (or angular velocity). From this energy flux,  $n_0F_J$  is used to keep the outer planet and its coorbital region nearly circular (see Figure 5; here,  $n_0$  is the outer planet's mean motion). The remaining energy flux,  $(n_i - n_o)F_J$ , is dissipated in the outer planet's coorbital region. Reciprocally, a fraction of the negative inward flux of angular momentum carried by the inner wake of the outer planet can be deposited in the inner planet's coorbital region and subsequently transmitted to the inner planet. Again, this exchange is associated with energy dissipation in the disk at a rate equal to the (absolute value of) the product of the flux of angular momentum transmitted to the inner planet by the outer one and the difference in the planets angular velocities. This dissipation occurs, as is usual in diskplanet interactions, through the tidally excited density waves steepening into shocks (e.g., Goodman & Rafikov 2001). Numerically, shocks are dealt with through a combination of numerical diffusion and the application of an artificial viscosity. As a locally isothermal equation of state is adopted in our simulations, this dissipated energy is effectively lost to the system through cooling. While the total orbital energy of the two planets is dissipated due to the wake-planet interactions described above, their total angular momentum remains unaltered. As studied in the context of star-planet tidal interactions, energy dissipation at constant angular momentum leads to the divergent evolution of a planet pair (Papaloizou 2011; Lithwick & Wu 2012; Batygin & Morbidelli 2013).

We now derive an equation satisfied by the period ratio of the two planets as a direct consequence of considering the evolution of their total orbital energy and angular momentum. We denote by  $a_i$ ,  $e_i$  and  $M_i$  the semi-major axis, eccentricity and mass of the inner planet (with the subscript changed to o denoting the same quantities for the outer planet). The total

angular momentum of the two planets is

$$J = J_{\rm i} + J_{\rm o} = M_{\rm i} \sqrt{G M_{\star} a_{\rm i} (1 - e_{\rm i}^2)} + M_{\rm o} \sqrt{G M_{\star} a_{\rm o} (1 - e_{\rm o}^2)},$$

which gives, correct to second order in the eccentricities,

$$\dot{J} \equiv \frac{dJ}{dt} = J_{\rm i} \left( \frac{\dot{a}_{\rm i}}{2a_{\rm i}} - e_{\rm i} \dot{e}_{\rm i} \right) + J_{\rm o} \left( \frac{\dot{a}_{\rm o}}{2a_{\rm o}} - e_{\rm o} \dot{e}_{\rm o} \right). \label{eq:Jacobs}$$

We are looking for changes in the planets' semi-major axes and eccentricities that occur on similar timescales, we may therefore discard the eccentricity terms in the expressions for  $\dot{J}$ ,  $J_{\rm i}$  and  $J_{\rm o}$ . Denoting by  $\Gamma_{\rm i}$  and  $\Gamma_{\rm o}$  the torques exerted by the disk on the inner and outer planets, respectively, conservation of angular momentum reads

$$\dot{J} = J_{\rm i} \frac{\dot{a}_{\rm i}}{2a_{\rm i}} + J_{\rm o} \frac{\dot{a}_{\rm o}}{2a_{\rm o}} = \Gamma_{\rm i} + \Gamma_{\rm o}.$$
 (1)

The total orbital energy is given by

$$E = -\frac{GM_{\star}M_{\rm i}}{2a_{\rm i}} - \frac{GM_{\star}M_{\rm o}}{2a_{\rm o}},$$

and conservation of energy reads

$$\dot{E} = \frac{GM_{\star}M_{i}}{2a_{i}^{2}}\dot{a}_{i} + \frac{GM_{\star}M_{o}}{2a_{o}^{2}}\dot{a}_{o} 
= n_{i}\Gamma_{i} + n_{o}\Gamma_{o} - \frac{GM_{\star}M_{i}e_{i}^{2}}{a_{i}\tau_{c,i}} - \frac{GM_{\star}M_{o}e_{o}^{2}}{a_{o}\tau_{c,o}} - |\dot{E}|_{\text{wake}}, (2)$$

where  $n_{\rm i,o} = \sqrt{GM_{\star}/a_{\rm i,o}^3}$  the planets mean motion. Here the right hand side of Eq. (2) contains three contributions. The first arises from the energy dissipation in the disk resulting from the action of the torques  $\Gamma_{i,o}$ . As these are negative this energy is removed from the orbital motion. The second originates from orbital circularization due to diskplanet interactions. The quantities  $\tau_{c,i}$  and  $\tau_{c,o}$  are the circularization times for the planets that arise from the disk torque and energy dissipation acting on each planet through the effects of its own wake (Nelson & Papaloizou 2002; Papaloizou & Szuszkiewicz 2005). The third and final contribution  $-|\dot{E}|_{\text{wake}}$  stems from the energy dissipation due to wake-planet interactions. We remark that wake dissipation in the coorbital region of the outer planet contributes  $(n_i - n_o)|F_J|$  to  $|E|_{\text{wake}}$ , in addition to a corresponding contribution arising from the coorbital region of the inner planet, as indicated above. Note that terms of order  $e_{i,0}^2$  are retained above even though the eccentricities are small as it is assumed that  $\tau_{i,o}$  are small enough so that dissipation through circularization could be as important as, or even dominate the other effects under some circumstances.

Combining Eqs. (1) and (2), we find

$$\frac{1}{3} \frac{n_{o}}{n_{i}} \frac{d}{dt} \left( \frac{n_{i}}{n_{o}} \right) = \left( \frac{\Gamma_{o}}{J_{o}} - \frac{\Gamma_{i}}{J_{i}} \right) + \frac{J_{i} + J_{o}}{J_{i} J_{o} (n_{i} - n_{o})} \left( n_{i} J_{i} \frac{e_{i}^{2}}{\tau_{c,i}} + n_{o} J_{o} \frac{e_{o}^{2}}{\tau_{c,o}} + |\dot{E}|_{\text{wake}} \right).$$
(3)

When wake-planet interactions are negligible ( $|\dot{E}|_{\rm wake}=0$ ), Eq. (3) shows that, far from resonance, where the eccentricities are very small, the planet's period ratio  $n_{\rm i}/n_{\rm o}$  decreases as a consequence of convergent migration, provided that  $\Gamma_{\rm o}/J_{\rm o} < \Gamma_{\rm i}/J_{\rm i}$ . As expected, the latter condition is that

the inward migration rate of the outer planet should exceed the inward migration rate of the inner planet. As the eccentricities increase as resonance is approached, a steady state may be reached in which the planets period ratio and eccentricities take stationary values. If the eccentricity damping timescales are sufficiently short, disk-driven circularization of the orbits can reverse convergent migration, that is the planets period ratio can increase.

Eq. (3) highlights that wake-planet interactions may also lead to divergent evolution of a planet pair. Divergent evolution driven by wake-planet interactions does not require the planets to be resonantly coupled, as already inferred from the simulations shown in Figure 5. Similar divergent evolution of a non-resonant planet pair embedded in a disk, comprising a Jupiter and a super-Earth, was reported by Podlewska-Gaca et al. (2012). When divergent evolution is primarily due to wake-planet interactions, as the period ratio of the planet pair increases away from a resonant value, the distance to resonance increases, and the forced eccentricities therefore decrease (e.g., Papaloizou 2011). It implies that orbital circularization is a natural consequence of divergent evolution driven by wake-planet interactions. This is actually a major difference between the divergent evolutions driven by wake-planet interactions and by orbital circularization (through the disk or stellar tides): eccentricity damping is the consequence of the former mechanism, while it is the cause of the latter. Note that, with both mechanisms, the divergent evolution of a resonant planet pair maintains the libration of the resonant angles by damping the eccentricities.

We call disk-driven resonant repulsion the divergent evolution of a resonant planet pair embedded in a disk, following the terminology introduced by Lithwick & Wu (2012) for the divergent evolution of a resonant planet pair due to star-planet tidal interactions. We stress that disk-driven resonant repulsion can have two origins: (i) disk circularization of the orbits and (ii) wake-planet interactions. In other words, disk-driven repulsion comprises (i) circularization-driven repulsion and (ii) wake-driven repulsion. The results of hydrodynamical simulations shown above indicate that, for the disk and planet parameters that we have considered, wake-planet repulsion dominates circularization-driven repulsion. This point will be further illustrated in Sect. 3.2.1.

When is wake-driven repulsion important?— We have seen above that the period ratio of a planet pair embedded in a disk may increase due to angular momentum transfer between the planets through their wakes. We further discuss in this paragraph under what conditions wake-planet interactions may lead to efficient divergent evolution of a planet pair. We separate the planet pair into a donor and a recipient. The bigger the donor's mass, the stronger its wake, and the easier for the wake to deposit angular momentum in the coorbital region of the recipient planet through the dissipation of shocks. This requires the dimensionless parameter  $q/h^3$  of the donor planet to typically exceed unity (q) is the planet-to-star mass ratio and h the disk's aspect ratio). The donor planet can thus be a partial or a deep gap-opening planet. The angular momentum that is deposited by the donor's wake is (at least partly) transferred to the recipient planet through an effective corotation torque (Podlewska-Gaca et al. 2012). If the recipient's mass is too big, the density in its coorbital region will be too low for this effective corotation torque to matter. In other words, the recipient could be a partial gap-opening planet or even a typeI migrating planet. These considerations show why divergent evolution is neither expected for two type-I migrating planets (the donor's wake being too weak), nor for two type-II migrating planets (the recipient's gap being too deep). We have checked this with hydrodynamical simulations, not illustrated here

The above considerations also help understand the different rates of divergent evolution obtained in Figure 2. The fact that both planets open a partial gap is a favorable situation for wake-planet interactions to play a significant role. In the top row of panels, where the planets become locked in the 2:1 MMR, the high-density region between the two gaps (see upper panel in Figure 3) causes significant deposition of angular momentum in the planets coorbital region and therefore very efficient divergent evolution. In contrast, in the bottom row of panels, where the planets merge their gap and become locked in the 3:2 MMR, the moderate disk density left between the planets can only trigger slow divergent evolution. In the middle row of panels, where the period ratio stalls near 1.7, a steady state is reached with background convergent migration balanced by wake-planet divergent evolution.

Evolution towards a steady state— When the planets are widely separated, they are expected to interact with the disk independently of each other and they can then enter a convergent migration phase. As they approach each other both planet-planet interactions, and wake-planet interactions where the planets interact with each others wakes can occur. Both these processes involve exchanges of orbital energy and angular momentum between the planets. Planet-planet interactions can result in resonant trapping associated with the growth of eccentricities, while wake-planet interactions act to produce divergent migration without the growth of eccentricities. From Eq. (3) we see that both circularization- and wake-driven resonant repulsions act together to increase the period ratio. If wake-driven repulsion dominates after the eccentricities have damped to low values, with  $|\dot{E}_{\text{wake}}|$  remaining constant, the period ratio should increase linearly with time, which is roughly what is obtained in the simulation presented in the top row of panels in Figure 2. However, in the longer term  $|\dot{E}_{\text{wake}}|$  should decrease with time as the planets separate, which indicates that a steady state should be ultimately reached with convergent migration driven by background disk torques balancing wake-driven repulsion. We stress that wake-planet interactions cause a non-linear evolution of the disk's density profile near the planets, which may affect the time evolution of the background torques responsible for convergent migration. At least in the simulation without planet-planet interaction of Figure 5, a slow decrease in the background torques could explain why the period ratio decreases then increases, instead of reaching a stationary nonresonant value. Another possibility is that convergent migration and disk-driven repulsion behave differently as the planet pair moves closer to the star, if the torques responsible for both mechanisms have different radial dependences. Investigation of these aspects is deferred to a future study.

#### 2.2.3. Disk dispersal model

The above simulations of the Kepler-46 system show that the planets' period ratio can take a range of values, depending on the convergent migration rate during the early evolution of the system. The limited duration of the simulations (up to a few thousand orbits) and the fact that planets still migrate at the end of the simulations however raise the question of the long-term evolution of the system. Even when the inward migration of the planets gets stalled<sup>1</sup>, further evolution of the period ratio can be maintained by disk-driven resonant repulsion. A steady state may a priori be achieved after depletion of the protoplanetary disk. Disk dispersal typically occurs between 10<sup>6</sup> and 10<sup>7</sup> years after formation of the central star. Photoevaporation driven by extreme ultraviolet radiation from the star opens a gap in the disk at separations of typically a few AU for Sun-like stars (e.g., Owen et al. 2010; Alexander & Pascucci 2012). For planets below that separation the background disk will be depleted on up to a viscous timescale at the orbital separation where photoevaporation sets in. Assuming a local viscous alpha parameter of a few  $\times 10^{-3}$ , viscous draining of the inner disk could operate in a few 10<sup>4</sup> years, that is typically a few 10<sup>5</sup> orbital periods at the present location of Kepler-46b and Kepler-46c.

To assess the impact of disk evaporation on our results, we have restarted two simulations adopting a simple exponential decay of the surface density profile. This is done by solving  $\partial_t \Sigma = -(\overline{\Sigma} - \Sigma_{target})/\tau_{evap}$  in addition to the hydrodynamical equations, where  $\overline{\Sigma}$  is the azimuthally-averaged density profile at restart time (from which evaporation switches on),  $\Sigma_{target} = 10^{-3}\overline{\Sigma}$  is an arbitrarily small density profile in a steady state (taken to be not zero for numerical convenience), and  $\tau_{evap}$  is the evaporation timescale. For illustrative purposes, we have considered three short evaporation timescales: 100, 500 and 2000 orbits, simulations being restarted at 1000 orbits. Results are shown in Figure 6.

The upper panels are obtained with  $M_{\rm inner}=0.4M_{\rm J}$  and  $\Sigma_0=3\times10^{-4}$ , for which a rapid divergent evolution occurs after capture in the 2:1 MMR. We see that the evolution is frozen out at a few evaporation timescales after restart, the planets reaching stationary eccentricities and semi-major axes. Similarly, the lower panels in Figure 6 show the results for  $M_{\rm inner}=0.6M_{\rm J}$  and  $\Sigma_0=6\times10^{-4}$ , for which convergent migration stalls at about the observed period ratio in the Kepler-46 system. In that case, including disk evaporation stalls the migration of both planets, as expected, but it does not significantly affect the planets eccentricities and period ratio. The final period ratio remains very close to the observed value.

# 3. APPLICATION TO KEPLER'S MULTI-PLANETARY SYSTEMS

## 3.1. *Introduction and strategy*

In Section 2 we have presented results of hydrodynamical simulations modeling the early evolution of Kepler-46b and Kepler-46c as they were embedded in their parent protoplanetary disk. The variety of period ratios obtained in our simulations raises the question of whether disk-planets interactions could partly explain the diversity of period ratios in Kepler's multi-planetary systems. We review below some of the processes that might account for such diversity.

#### 3.1.1. Tidally-driven resonant repulsion?

As highlighted in Figure 1, Kepler's multi-planetary systems show a clear tendency for planet pairs near resonances

<sup>&</sup>lt;sup>1</sup> This could be the case for instance when the mass of the disk inside the inner planet becomes smaller than the mass of the two gap-opening planets, a migration regime known as planet-dominated type II migration.

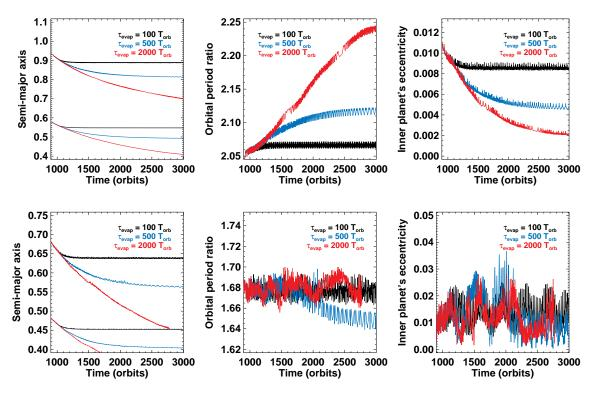


Figure 6. Time evolution of the planets' semi-major axis, period ratio and eccentricity (for the inner planet only) with a simple model for disk dispersal (see text). Disk dispersal is switched on at 1000 orbits and the evaporation timescale ( $\tau_{\text{evap}}$ ) is varied from 100 to 2000 orbits. Results in the upper panels are for  $M_{\text{inner}} = 0.4 M_{\text{J}}$  and  $\Sigma_0 = 3 \times 10^{-4}$ . Results in the lower panels are for  $M_{\text{inner}} = 0.6 M_{\text{J}}$  and  $\Sigma_0 = 6 \times 10^{-4}$ .

to feature period ratios slightly greater than strict commensurability. Divergent evolution of a short-period resonant planet pair due to star-planet tidal interactions could partly explain this feature (Lithwick & Wu 2012; Batygin & Morbidelli 2013). Although the efficiency of tidal dissipation remains largely uncertain, it is thought that efficient tidal circularization requires the inner planet to orbit its star in less than a few days. As can be seen in Figure 1 many of Kepler's candidate systems have an inner planet beyond 10 days, for which tidal circularization is unlikely to have caused significant resonant repulsion (see Section A of the appendix). For these systems we propose that resonant repulsion driven by disk-planets interactions could have played a prominent role in determining the observed period ratios.

## 3.1.2. *Disk-driven type I migration?*

The vast majority of the planets in Kepler's multi-planetary systems have physical radii between 0.1 and 0.3 Jupiter radii, which places them in the super-Earth to Neptune-mass range. From the mass-radius diagram of Kepler candidates followed up by radial velocity, the median mass of a 0.2 Jupiter-radius planet is about 10 to 15 Earth-masses (see, e.g., http://exoplanets.org). Based on generally considered temperatures and viscosities in protoplanetary disks (corresponding to h=0.05 and  $\alpha\sim {\rm a~few}\times 10^{-3})$  such planets are expected to experience type I migration. Recent N-body experiments by Rein (2012) have shown that convergent migration of type-I migrating planets yields very little departure from strict commensurability in contrast with Kepler's data. He showed that the inclusion of stochastic forces in addition to type I migration could reproduce the observed distribution of period ratios quite nicely. Such agreement has been obtained assuming that the initial period ratio distribution is the observed one, and taking the same convergent migration timescale and the same amplitude of stochastic forces for all Kepler's multiple systems, which remains quite uncertain given the expected diversity of physical properties in protoplanetary disks. Still, his results indicate that type I migration alone may not be able to account for Kepler's diversity of period ratios.

#### 3.1.3. Disk-driven repulsion of partial gap-opening planets?

Based on our results of hydrodynamical simulations for the Kepler-46 system, we propose that some of Kepler's planet candidates in multi-planetary systems could have opened partial gaps in their parent disk, thereby escaping the type I migration regime. This could be the case if, for instance, planets formed and/or migrated in regions of low turbulent activity (dead zones; see, e.g., Fleming & Stone 2003) or if the disk's aspect ratio takes smaller values than commonly adopted. Aspect ratios  $\lesssim 3\%$  are likely typical of the short orbital separations at which Kepler's candidate systems are detected. To address this possibility, we carried out hydrodynamical simulations with two planets in the super-Earth mass range. The inner planet's mass  $M_{\rm inner} = 15 M_{\oplus}$ , the outer planet's mass  $M_{\rm outer}=13M_{\oplus}$  and the central star is one Solar mass. The planet-to-primary mass ratios are therefore  $q_{\text{inner}} = 4.4 \times 10^{-5}$  and  $q_{\text{outer}} = 4 \times 10^{-5}$ , that is an order-ofmagnitude smaller than those of Kepler-46b (median value) and Kepler-46c. In order to get similar gap depths in the super-Earths and Kepler-46 simulations, we adopted values of h and  $\alpha$  such that the dimensionless parameters in the gapopening criterion of Crida et al. (2006) take the same values. For the super-Earths simulations, this yields h = 0.023 and  $\alpha = 2.3 \times 10^{-3}$ . All other simulation parameters are other-

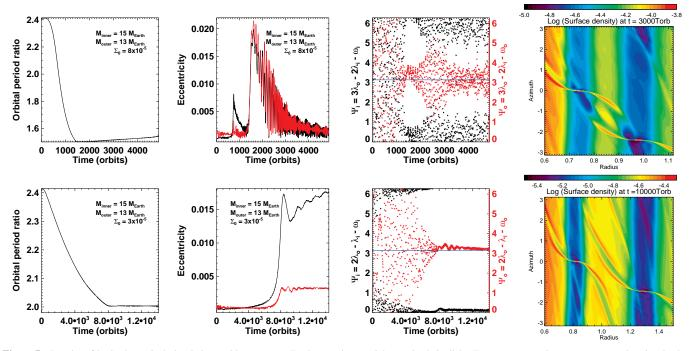


Figure 7. Results of hydrodynamical simulations with two super-Earths opening partial gaps in their disk. Top row: case where convergent migration leads to capture into the 3:2 MMR followed by rapid divergent evolution. Bottom row: slow convergent migration leading to capture into the 2:1 MMR with no subsequent divergent evolution. From left to right, the panels display the time evolution of the planets orbital period ratio, eccentricities, relevant resonant angles, and a snapshot of the disk's surface density.

wise identical, except the grid resolution that we increased to  $600 \times 1200$ .

Figure 7 displays the results of two simulations. In the top panels, the unperturbed disk's surface density is  $\Sigma_0$  =  $8 \times 10^{-5}$ . We see that the planets lock themselves in the 3:2 MMR from about 1300 orbits. Divergent evolution proceeds with a decrease in the planets eccentricities. After reaching exactly 1.5 at about 1500 orbits, the period ratio increases to 1.54 at 5000 orbits. As illustrated by the screenshot of the disk surface density, the proximity of the planets allows their wakes to penetrate into each others coorbital region, where they can deposit part of their angular momentum flux. As we have shown in Section 2.2.2, transfer of angular momentum between planets through wake-planet interactions will result in a loss rate of the total orbital energy of the two planets. This has the consequence of increasing the period ratio and decreasing the eccentricities. In the bottom panels of Figure 7, the unperturbed disk surface density parameter is decreased to  $\Sigma_0 = 3 \times 10^{-5}$ . Here, convergent migration due to the background disk torques is slow enough to lock the planets in the 2:1 MMR, but this time the resonant capture does not lead to divergent evolution. Instead, a steady state is reached in which both the eccentricities and the orbital period ratio take stationary values. This steady state is a consequence of negligible wake-planet interactions in this case. As illustrated in the bottom-right panel of Figure 7, the planets are sufficiently far from each other that their wakes primarily transfer energy and angular momentum to regions of the disk that are not coorbital with the planets.

## 3.2. Customized three-body simulations

The results of Section 3.1.3 support the idea that disk-driven resonant repulsion of partial gap-opening super-Earths may lead to period ratios that substantially differ from nominal resonant values. As shown in Section 2.2.2, this mechanism has

two origins: circularization of the orbits and wake-planet interactions. Its efficiency depends on the planets masses and the evolution of the disk's surface density. The survey of such a large parameter space is out of reach of hydrodynamical simulations, but three-body simulations with customized prescriptions for migration, eccentricity damping and disk dispersal can help illustrate the diversity of period ratios that can be achieved. This is the strategy that we have adopted. For illustration purposes we have considered fixed planet masses:  $M_{\rm inner} = 15 M_{\oplus}$ ,  $M_{\rm outer} = 13 M_{\oplus}$  and  $M_{\star} = M_{\odot}$  (as in Section 3.1.3).

#### 3.2.1. *Method*

Our three-body simulations solve the equations of motion for the two planets and the central star using a standard technique. Planets are assumed to be coplanar. Disk-planet interactions are incorporated by applying appropriate dissipative forces (for details, see Papaloizou 2011). Inspection at Eq. (3) shows that, in order to model the planets evolution, we need to specify (i) the rate of convergent migration before disk-driven repulsion sets in, (ii) the damping rate of the eccentricities, (iii) the efficiency of wake-driven divergent evolution, and (iv) how disk dispersal is modeled. Point (iii) remains uncertain at this stage, as the term  $|\dot{E}_{\text{wake}}|$  in the righthand side of Eq. (3), which models energy dissipation due to wake-planet interactions, should depend sensitively on the planet masses, their mutual separation and distance from the central star, and several disk quantities (including its temperature and viscosity). A systematic study of this dependence goes beyond the scope of this paper, and is therefore left for future work. In order to do simple modeling, and to minimize the number of free parameters, we do not attempt to parameterize the  $|\dot{E}_{\text{wake}}|$  term. Instead, we model disk-driven repulsion as circularization-driven repulsion only. In other words, in Eq. (3) we compensate the absence of the  $|\dot{E}_{\text{wake}}|$ 

= 13  $M_{Earth}$  $\Sigma_0 = 8 \times 10^{-5}$ 

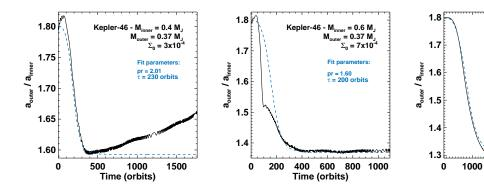
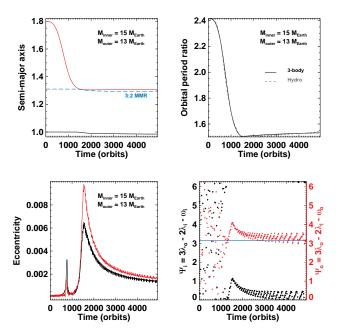


Figure 8. Time evolution of the ratio of planets semi-major axis obtained in three hydrodynamical simulations (solid curves). The planet masses and the unperturbed surface density parameter  $\Sigma_0$  are indicated in the top-right corner of each panel. The dashed curves display our fitting formula for the planets convergent migration prior to disk-driven resonant repulsion, given by Eq. (4).



**Figure 9.** Results of a three-body simulation with prescribed convergent migration and eccentricity damping. The expression given by Eq. (4) is used for convergent migration with  $\tau=1000$  orbits and pr = 1.5. The eccentricity damping timescale is 20 orbital periods. The dashed grey curve in the topright panel shows the period ratio obtained in the hydrodynamical simulation of  $\S$  3.1.3 with  $\Sigma_0=8\times10^{-5}$ .

term in our three-body integrations by considering circularization timescales  $\tau_{c,i}$  and  $\tau_{c,o}$  that are shorter than in the hydrodynamical simulations. Damping of the planets' eccentricity is modeled as an exponential decay with a constant damping timescale to orbital period ratio, which we take as a free parameter (specified below).

To model the convergent migration prior to resonant repulsion, we adopt a simple prescription that reproduces the results of hydrodynamical simulations. Denoting by R the ratio of semi-major axes ( $R = a_{\text{outer}}/a_{\text{inner}}$ ), we found good agreement using

$$R(t) = R(t=0) \times 10^f \tag{4}$$

with

$$f = \log_{10} \left[ \frac{(\text{pr})^{2/3}}{R(t=0)} \right] \times \frac{(t/\tau)^3}{\sqrt{1 + (t/\tau)^6}},$$
 (5)

where pr and  $\tau$  are fitting parameters. The expression in Eq. (4) tends to a constant value for  $t \gg \tau$ , which mimics the fact that convergent migration is found to nearly stall before resonant repulsion sets in. In Eq. (5), pr denotes the period ratio at which convergent migration approximately stalls, and  $\tau$  the time at which this occurs. The good agreement between this migration prescription and our hydrodynamical simulations is illustrated in Figure 8. Note that in the three-body simulations, disk-driven migration is applied to the outer planet only.

2000

Time (orbits)

3000

4000

We display in Figure 9 the results of a three-body simulation with pr = 1.50 and  $\tau = 1000$  orbits, which mimics the convergent migration obtained in the hydrodynamical simulation of Section 3.1.3 with  $\Sigma_0 = 8 \times 10^{-5}$  (see right panel of Figure 8). In the top-left panel of Figure 9, only the semimajor axis of the outer planet varies in the first 1500 orbits as our prescription for disk-driven migration is applied to the outer planet. Once resonant repulsion sets in near 1500 orbits, the semi-major axis of the inner planet decreases slightly, that of the outer planet increases slightly as well. The eccentricity damping timescale here is 20 planet orbits, and this rather short timescale is found to give very similar divergent evolutions in the three-body and hydrodynamical simulations (see top-right panel in Figure 9). At 5000 orbits, the period ratio is 1.53 in the three-body run, and 1.54 in the hydrodynamical run. This small difference can be qualitatively explained by the fact that the repulsion occurs at a slightly larger pace in the hydrodynamical simulation than has been modelled in the three-body run. Furthermore, we point out that the eccentricity peaks near the 2:1 and 3:2 MMRs are about a factor of 2 to 3 smaller in the three-body simulation (compare with the eccentricities of the hydrodynamical run shown in the second upper panel of Figure 7). The reason for this difference is most likely a reflection of the fact that the actual circularization time in the hydrodynamical run is longer than that adopted in the three-body integration, consistent with the operation of wake-planet repulsion in addition to circularizationdriven repulsion as discussed above.

We also incorporated a simple model for disk dispersal, which is taken to occur between  $10^4$  and  $10^6$  orbits. Since planets are assumed to be already formed at the beginning of the simulations, this range of timescales is meant to account for different planet formation timescales. The longest time ( $10^6$  orbits) corresponds to a case where both planet formation and capture into resonance following convergent migration occur rapidly. The shortest one ( $10^4$  orbits) stands for

the opposite. Once disk dispersal switches on, the eccentricity damping timescale is progressively increased as an exponential growth with characteristic timescale  $\tau_{\rm evap}=2000$  orbits. This timescale is shorter than the typical viscous draining timescale of a disk inside the photoevaporation radius. It implies that the efficiency of disk-driven resonant repulsion is nearly entirely determined by the time from the beginning of the simulations at which dispersal switches on.

#### 3.2.2. Results

We display in Figure 10 the results of a series of three-body simulations using the model described in Section 3.2.1. Recall that  $M_{\text{inner}} = 15 M_{\oplus}$ ,  $M_{\text{outer}} = 13 M_{\oplus}$  and  $M_{\star} = M_{\odot}$ , which can be thought of being representative of Kepler's sample of multi-planetary systems (the planets' mass ratio is arbitrary, it takes the same value as in the hydrodynamical simulations in Section 3.1.3). Planets are initiated with a period ratio of 2.4. The prescription for convergent migration given at Eq. (4) is used with pr = 1.50 and  $\tau = 1000$  orbits. This value of pr is meant to explore the diversity of period ratios that can be achieved by disk-driven resonant repulsion away from the 3:2 MMR. The eccentricity damping timescale is varied from 20 to 200 orbits, and the time at which disk dispersal switches on from  $10^4$  to  $10^6$  orbits (see Section 3.2.1). Given the duration of disk-driven resonant repulsion, our results are found to have very little dependence on the "convergent migration timescale"  $\tau$ . Simulations were carried out over  $1.2 \times 10^6$ orbits, and the period ratio time-averaged over the last 1000 orbits of the simulations is indicated by the color bar. For a given eccentricity damping timescale, the later disk dispersal occurs, the longer planets eccentricities are damped, and therefore the larger the final period ratio. At a given time prior to disk dispersal, the shorter the eccentricity damping timescale, the larger the final period ratio, again as expected. For the shortest damping timescales that we have considered, period ratios can reach  $\sim 1.75$ . With such short timescales, planets can evolve continuously from the 3:2 MMR to the 2:1 MMR (that is, the 2:1 resonant angles start to librate when the 3:2 resonant angles no longer librate). Had we taken even shorter damping timescales or delayed disk dispersal even more, resonant repulsion would have led to period ratios exceeding 2.

The main conclusion that can be drawn from Figure 10 is that partial gap-opening super-Earths may experience significant disk-driven resonant repulsion away from the nominal 3:2 MMR. Under very favorable circumstances (particularly efficient repulsion maintained over a particularly long timescale) period ratios can easily exceed nominal resonant values. Although we have considered fixed planet masses for illustration purposes, we believe that disk-driven resonant repulsion is a generic mechanism that may have likely occurred among Kepler's multi-planetary systems.

## 4. CONCLUDING REMARKS

The multi-planetary systems detected by the Kepler mission have very diverse architectures, which reflect the wide range of conditions under which planets may form and evolve. The quasi-coplanar orbits in Kepler's multiple systems suggest that interactions between planets and their parent protoplanetary disk should play a prominent role in shaping such diverse architectures. In particular, close planet pairs feature a variety of orbital period ratios and many of them are not in mean-motion resonance. Convergent migration of multi-

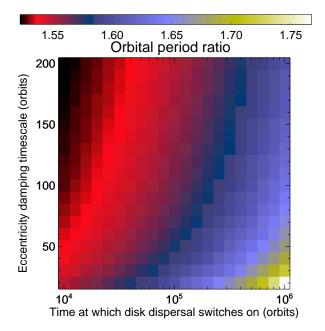


**Figure 10.** Results of three-body simulations with prescribed convergent migration and eccentricity damping. The central star has a Solar mass. The mass of the inner and outer planets is  $M_{\rm inner} = 15 M_{\rm Earth}$  and  $M_{\rm inner} = 13 M_{\rm Earth}$ , respectively. Convergent migration is modeled using the expression in Eq. (4) with pr = 1.5 and  $\tau = 10^3$  orbits. The eccentricity damping timescale is varied from 20 to 200 orbits (y-axis), and it remains fixed until disk dispersal is switched on. The timescale at which disk dispersal switches on ranges from  $10^4$  to  $10^6$  orbits after the beginning of the simulations (x-axis), and the evaporation timescale is set to 2000 orbits. The orbital period ratio obtained after  $1.2 \times 10^6$  orbits, and time-averaged over the last 1000 orbits, is colour-coded.

ple planets due to disk-planet interactions may lead to resonant systems in disks where turbulence is low enough not to disrupt resonances (Ketchum et al. 2011; Pierens et al. 2011; Rein 2012). Resonant planet pairs formed by disk-planet interactions may experience divergent evolution of their orbits due to tidal orbital circularization (Papaloizou & Terquem 2010; Papaloizou 2011). This so-called *tidal resonant repulsion* may increase the orbital period ratio of close-in planet pairs quite substantially depending on the efficiency of starplanet tidal interactions (Papaloizou 2011; Lithwick & Wu 2012; Batygin & Morbidelli 2013). Tidal resonant repulsion could help account for the diversity of period ratios in Kepler's close-in planet pairs.

We have shown in this paper that disk-planets interactions could also form planet pairs with a variety of period ratios. We have first focused on the Kepler-46 planetary system, in which the two Saturn-mass planets Kepler-46b and Kepler-46c have a period ratio  $\approx 1.69$  (Nesvorný et al. 2012). We have presented results of hydrodynamical simulations modeling the early evolution of these planets as they were embedded in their parent disk. For typical disk temperatures and turbulent viscosities, both planets are expected to open a partial gap around their orbit. A rapid convergent migration causes the planets to merge their gaps and to evolve into a common gap. Depending on the density's structure inside the common gap, the planets' convergent migration is found to stall with a variety of period ratios between 1.5 and 1.7 (see Figure 4). The observed period ratio of Kepler-46b/c can be reproduced without the planets being in mean-motion resonance.

Our results also highlight that disk-planets interactions may significantly increase the orbital period ratio of a planet pair

from a near-resonant value, a mechanism that we term diskdriven resonant repulsion. It has two origins: (i) orbital circularization by the disk, and (ii) the interaction between each planet and the wake of its companion. As the wake of a planet turns into a shock at some distance from the planet, it may deposit angular momentum in the coorbital region of another planet through an effective corotation torque. We have shown that this mechanism can dissipate the total orbital energy of a planet pair without changing its total angular momentum, a configuration that increases the planets' period ratio and decreases their eccentricity. Resonant repulsion caused by wake-planet interactions can be particularly efficient when at least one of the planets opens a partial gap around its orbit (see Section 2.2.2). For the disk and planet parameters adopted in this work, wake-planet interactions are much more efficient at driving the repulsion of a planet pair than disk circularization. However, there may be circumstances for which this balance is different.

The strength of wake-planet interactions increases as the radial separation between planets decreases, independently of their eccentricity. If wake-planet interactions are the dominant process for the divergent evolution of a planet pair, then one could expect the period ratio to reach a constant value, which could be different from a resonant ratio. Our results of simulations report, however, many cases where the period ratio nearly stalls but then increases. There could be two reasons for this behavior. First, wake-planet interactions cause a (non-linear) evolution of the disk's density profile near the planets, which causes the torques driving convergent migration and wake-planet interaction to change over time. Furthermore, independently of the previous consideration, preliminary results indicate that the torques responsible for convergent migration and for wake-driven repulsion have different dependences on the stellar distance as the planets migrate. Both effects are found to strengthen wake-driven repulsion as compared to convergent migration as planets migrate inwards. This would explain why, in our simulations, the period ratio of inwardly migrating planet pairs increases after reaching a nearly constant value. The above considerations indicate that wake-planet interactions may naturally increase the period ratio of planet pairs away from resonant values.

One of our low-mass disk models for Kepler-46, in which the Saturn-mass planets are captured in the 2:1 MMR, a period ratio of 2.3 is attained in as short as a few thousand orbits. We note that a significant divergent evolution of sub-Jovian planets was obtained in some of the hydrodynamical simulations of Rein et al. (2010) and Rein et al. (2012). The similarity between their results of simulations and ours (convergent migration nearly stalled close to resonance, followed by divergent evolution of the planets orbits alongside the damping of their eccentricity) suggests that the divergent evolution obtained in these simulations is likely to arise from wake-planet interactions.

Many planets in Kepler's multiple systems are in the super-

Earth to Neptune-mass range, and have orbital periods below 100 days. At these short periods the aspect ratio of a disk should be rather small, thus many Kepler's planet candidates could have opened partial gaps in their parent disk. In contrast to the Saturn-mass planets in the Kepler-46 system, super-Earths are not expected to merge their gaps and to evolve in a common gap, unless a very fast convergent migration brings them to very short mutual separations. We have argued instead that close-in super-Earths are good candidates for efficient resonant repulsion caused by wake-planet interactions. For instance, one of our simulations shows that the orbital period ratio of two  $\sim$  15 Earth-mass planets increases from 1.5 to 1.55 in few thousand orbits. Disk-driven repulsion via wake-planet interactions could explain why many planet pairs in Kepler's multiple systems have period ratios slightly greater than resonant. While resonant repulsion driven by stellar tides should only be relevant to planet pairs with orbital periods below a few days, disk-driven repulsion may also apply to planets on longer periods.

The TTV signals of Kepler's short-period planet pairs indicate that some of these planets have small but not zero free eccentricities (Lithwick et al. 2012). Free eccentricities get quickly damped by tidal orbital circularization. However, the presence of a disk of planetesimals or a non-smooth gas disk dispersal could give planets some free eccentricity. Close-in planet pairs that seem to have undergone resonant repulsion, but which have not zero free eccentricities, like Kepler-23b/c and Kepler-28b/c, could indicate that repulsion was primarily mediated by disk-planets interactions rather than by starplanet tidal interactions.

We foresee at least three directions to pursue work on disk-driven resonant repulsion. Firstly, the effects of disk turbulence, which we have modeled with a constant viscosity, need to be addressed carefully. The levels of stochastic fluctuations required to disrupt the process as planet masses decrease, and to produce some residual free eccentricity should be explored. Secondly, planet mass growth should be taken into account as it may also lead to some divergent evolution (Petrovich et al. 2013). Thirdly, a Monte-Carlo approach with three-body integrations using simple prescriptions for the effects of disk-planet interactions should be used to compare the distribution of orbital elements among Kepler's planet pairs with the synthetic distributions predicted by disk-driven resonant repulsion.

CB is supported by a Herchel Smith Postdoctoral Fellowship of the University of Cambridge. We thank Gwenaël Boué, Cathie Clarke, Jérôme Guilet, Cristobal Petrovich and Yanqin Wu for useful discussions. We also thank the referee for a very helpful report. Hydrodynamical simulations were performed on the Darwin Supercomputer of the University of Cambridge High Performance Computing Service using Strategic Research Infrastructure Funding from the Higher Education Funding Council for England.

#### **APPENDIX**

### A – EFFICIENCY OF TIDAL RESONANT REPULSION OF A PLANET PAIR

We show here that star-planet tidal interactions are unlikely to cause significant divergent evolution of two planets in the super-Earth mass range when the orbital period of the inner planet exceeds about 10 days. In the constant time lag model, taking tidal dissipation within the planet to be much larger than within the star, the orbital circularization timescale,  $\tau_{circ}$ , is given by equation

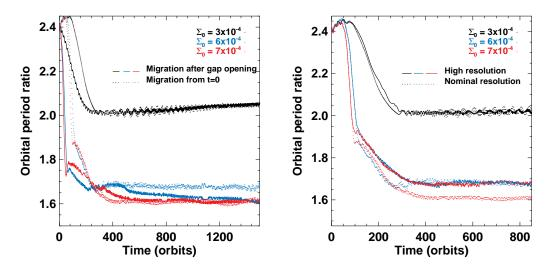


Figure 11. Ratio of orbital periods for  $M_{\text{inner}} = 0.6M_{\text{J}}$  and different values of the unperturbed surface density parameter  $\Sigma_0$ . The left panel compares our fiducial case where planets migrate from the beginning of the simulations (dotted curves) with the case where planets are first held on fixed circular orbits for 500 orbits before migrating (solid curves). The right panel shows the overall good convergence of our results when increasing the number of grid cells from  $400 \times 800$  (nominal resolution) to  $800 \times 1600$  (high resolution).

(25) of Goldreich & Soter (1966) and can be expressed as follows:

$$\tau_{\rm circ} = 4.5 \times 10^7 \, \rm yr \times \left(\frac{Q_{\rm i}'}{30}\right) \times \left(\frac{\rho_{\rm i}}{1 \, \rm g \, cm^{-3}}\right) \times \left(\frac{R_{\rm i}}{0.2 \, \rm R_{\rm Jup}}\right)^{-2} \times \left(\frac{M_{\star}}{M_{\odot}}\right)^{2/3} \times \left(\frac{T_{\rm i}}{10 \, \rm days}\right)^{13/3},\tag{A1}$$

where  $Q_i'$  is the tidal quality factor of the inner planet,  $\rho_i$  its mean density,  $R_i$  its physical radius,  $T_i$  its orbital period and  $M_{\star}$  is the star's mass. Divergent evolution of two resonant planets may occur as a result of tidal dissipation of orbital energy at approximately constant orbital angular momentum (Papaloizou 2011). The timescale for divergent evolution, which we denote by  $\tau_{\text{div}}$ , satisfies

$$\tau_{\rm div} \sim \frac{\tau_{\rm circ}}{e_{\rm i}^2} \times \frac{\Delta a}{a_{\rm i}},$$
(A2)

with  $a_i$  and  $e_i$  the semi-major axis and forced eccentricity of the inner planet, and  $\Delta a$  its change in semi-major axis during divergent evolution (it can be taken to be the planet's distance from resonance). We have  $e_i = C(M_o/M_\star) \times (\Delta a/a_i)^{-1}$ , where  $M_o = \mu M_i$  is the outer planet's mass,  $M_i$  the inner planet's mass ( $\mu$  denotes the outer-to-inner planet mass ratio), and C is a constant of order unity that varies with the resonance (see, e.g., equation 38 of Papaloizou 2011). Using Eq. (A1) and taking C = 1, we obtain

$$\tau_{\rm div} \sim 2 \times 10^{12} \, \rm yr \times \left(\frac{Q_{\rm i}^{'}}{30}\right) \times \mu^{-2} \times \left(\frac{\rho_{\rm i}}{1 \, \rm g \, cm^{-3}}\right)^{-1} \times \left(\frac{R_{\rm i}}{0.2 \, R_{\rm Jup}}\right)^{-8} \times \left(\frac{M_{\star}}{M_{\odot}}\right)^{8/3} \times \left(\frac{T_{\rm i}}{10 \, \rm days}\right)^{13/3} \times \left(\frac{\Delta a/a_{\rm i}}{10^{-2}}\right)^{3}. \tag{A33}$$

This order of magnitude estimate shows that planet pairs orbiting Sun-like stars should experience negligible tidally-driven resonant repulsion over gigayear timescales when the inner planet is a super-Earth, with  $R_i < 2R_{\oplus}$ ,  $\rho_i < 5 \, \mathrm{g \, cm^{-3}}$ , and orbital period greater or equal to 10 days, even if  $Q_i' = 1$  and  $\mu \gtrsim 1$ . Moreover, if the inner planet is a Jupiter-like planet, then assuming  $Q_i' \sim 10^5$  and  $\rho_i < 5 \, \mathrm{g \, cm^{-3}}$ , Eq. (A3) shows that divergent evolution of more than a few percent away from resonance is expected over a few gigayears as long as the inner planet's orbital period does not exceed 10 days.

## B - HYDRODYNAMICAL SIMULATIONS OF THE KEPLER-46 SYSTEM: ROBUSTNESS OF RESULTS

In the course of our numerical experiments, we have tested the robustness of our results by varying the assumptions made in the physical model and by varying the grid resolution.

Physical model— We performed several simulations reducing the disk's aspect ratio to 4% and 3% while keeping the same viscous alpha parameter. Although not illustrated here, these simulations show again a variety of outcomes, but none reproducing the observed period ratio between Kepler-46c and Kepler-46b. Decreasing the disk's aspect ratio makes the gaps carved by the planets deeper. When convergent migration is rapid enough for the planets to cross their 2:1 MMR and to evolve in a common gap, we find that the planets generally lock themselves into the 3:2, 4:3 or even 7:5 MMR with very little departure from exact commensurability. In these simulations, the density in the common gap is too low for wake-planet interactions to cause significant divergent evolution (see Section 2.2.2). These simulations thus suggest that partial gap opening is required to obtain a period ratio consistent with the observed value. Furthermore, as the structure of the gaps plays a prominent role in the final

evolution of the planets' period ratio, we carried out additional simulations where the planets were first held on fixed circular orbits for 500 orbits before migrating. This preliminary stage allowed enough time for each planet to build up a gap with a stationary density structure. The results of the simulations are shown in the left panel of Figure 11 for  $M_{\text{inner}} = 0.6M_{\text{J}}$  and three values of  $\Sigma_0$ . Starting with pre-evolved gaps changes the initial rate of convergent migration. Notwithstanding quite different initial evolutions, two out of these three models end up following the same evolution with or without pre-evolved gaps, and reach the same final period ratio at the end of the simulations. The model with  $\Sigma_0 = 6 \times 10^{-4}$  reaches a slightly smaller period ratio (decreased from 1.65 to 1.6 when starting with pre-evolved gaps).

Grid resolution— The effect of resolution was checked by doubling the number of grid cells along each direction for a few simulations. The results of three high-resolution runs ( $800 \times 1600$ ) are compared to the nominal-resolution runs ( $400 \times 800$ ) in the right panel of Figure 11. Doubling the grid resolution slightly changes the initial rate of convergent migration, leading to slightly different initial evolution. As for the above series of simulations with pre-evolved gaps, the model with capture into 2:1 MMR followed by resonant repulsion is not affected by doubling the resolution. The two models with common gap evolution seem again more susceptible to a variation in the initial convergent migration, but lead to small differences in the final outcome. Interestingly, both high-resolution models with  $\Sigma_0 = 6$  and  $7 \times 10^{-4}$  yield a period ratio  $\approx 1.68$ , in very good agreement with the observed value.

## **REFERENCES**

Alexander, R. D., & Pascucci, I. 2012, MNRAS, 422, L82
Baruteau, C., Fromang, S., Nelson, R. P., & Masset, F. 2011, A&A, 533, A84
Baruteau, C., & Masset, F. 2013, in Lecture Notes in Physics, Berlin Springer Verlag, Vol. 861, Lecture Notes in Physics, Berlin Springer Verlag, ed. J. Souchay, S. Mathis, & T. Tokieda, 201
Batalha, N. M., et al. 2013, ApJS, 204, 24
Batygin, K., & Morbidelli, A. 2013, AJ, 145, 1
Crida, A., Baruteau, C., Kley, W., & Masset, F. 2009, A&A, 502, 679
Crida, A., Morbidelli, A., & Masset, F. 2006, Icarus, 181, 587
Fleming, T., & Stone, J. M. 2003, ApJ, 585, 908
Gautier, III, T. N., et al. 2012, ApJ, 749, 15
Goldreich, P., & Soter, S. 1966, Icarus, 5, 375
Goodman, J., & Rafikov, R. R. 2001, ApJ, 552, 793
Ketchum, J. A., Adams, F. C., & Bloch, A. M. 2011, ApJ, 726, 53
Kley, W., & Crida, A. 2008, A&A, 487, L9
Lin, D. N. C., & Papaloizou, J. C. B. 1993, in Protostars and Planets III, ed.
E. H. Levy & J. I. Lunine, 749–835
Lissauer, J. J., et al. 2012, ApJ, 750, 112
—. 2011, ApJS, 197, 8
Lithwick, Y., & Wu, Y. 2012, ApJ, 756, L11
Lithwick, Y., Xie, J., & Wu, Y. 2012, ApJ, 761, 122

Masset, F. 2000, A&AS, 141, 165
Masset, F. S., & Papaloizou, J. C. B. 2003, ApJ, 588, 494
Mayor, M., et al. 2009, A&A, 507, 487
Murray-Clay, R. A., & Chiang, E. I. 2005, ApJ, 619, 623
Nelson, R. P., & Papaloizou, J. C. B. 2002, MNRAS, 333, L26
—. 2003, MNRAS, 339, 993
Nesvorný, D., Kipping, D. M., Buchhave, L. A., Bakos, G. Á., Hartman, J., & Schmitt, A. R. 2012, Science, 336, 1133
Owen, J. E., Ercolano, B., Clarke, C. J., & Alexander, R. D. 2010, MNRAS, 401, 1415
Papaloizou, J. C. B. 2011, Celestial Mechanics and Dynamical Astronomy, 111, 83
Papaloizou, J. C. B., & Szuszkiewicz, E. 2005, MNRAS, 363, 153
Papaloizou, J. C. B., & Terquem, C. 2010, MNRAS, 405, 573
Petrovich, C., Malhotra, R., & Tremaine, S. 2013, ApJ, 770, 24
Pierens, A., Baruteau, C., & Hersant, F. 2011, A&A, 531, A5
Podlewska-Gaca, E., Papaloizou, J. C. B., & Szuszkiewicz, E. 2012, MNRAS, 421, 1736
Rein, H. 2012, MNRAS, L526
Rein, H., Papaloizou, J. C. B., & Kley, W. 2010, A&A, 510, A4
Rein, H., Payne, M. J., Veras, D., & Ford, E. B. 2012, MNRAS, 426, 187